Optimisation of RNAV noise and emission abatement standard instrument departures

S. Hartjes and H. G. Visser
s.hartjes@tudelft.nl
Delft University of Technology
Delft, The Netherlands

S. J. Hebly
National Aerospace Laboratory NLR
Amsterdam, The Netherlands

ABSTRACT

In an effort to reduce the negative impact of civil aviation on the human environment, trajectory optimisation techniques have been used to minimise the single event impact of noise and gaseous emissions of departures on communities in the vicinity of airports. For this purpose, the earlier developed trajectory optimisation tool NOISHHH has been adapted to design departure trajectories optimised for environmental criteria, based on area navigation. The new version of NOISHHH combines a noise model, an emissions inventory model, a geographic information system and a dynamic trajectory optimisation algorithm to generate flight paths with minimised environmental impact. Operational constraints have been introduced to ensure that the resulting flight paths are fully compliant with the guidelines and regulations that apply to the design of standard instrument departures and the use of area navigation. To illustrate the capabilities of the new version of NOISHHH, two numerical examples are presented, which are both redesigns of standard instrument departures currently in use at Amsterdam Airport Schiphol.

NOMENCLATURE

D	aircraft drag
E	specific energy
EI	emission index
h	altitude
J	performance index
K	weighting factor
R	turn radius
s	ground track distance
t	time
T	thrust
V	true airspeed
W	aircraft weight
x	x-co-ordinate
y	y-co-ordinate
γ	flight path angle
Γ	throttle setting
μ	bank angle
σ	fuel flow
χ	heading angle

1.0 INTRODUCTION

Since February 2003 the noise caused by civil aviation around Amsterdam Airport Schiphol (AAS) is controlled by enforcing maximum yearly day-evening-night average noise levels (L_{den}) and night average noise levels (L_{night}) at a number of enforcement points in the vicinity of the airport. In 2007, AAS accommodated 440,000 commercial flight movements in compliance with these noise regulations. Since public awareness of the effects of aviation noise is growing, relaxation of the regulations in the near future is not likely. This, in combination with a projected growth to 510,000 flight

Paper No. 3525. Manuscript received 7 January 2010, revised version received 6 August 2010, accepted 26 August 2010.

https://doi.org/10.1017/S0001924000004243 Published online by Cambridge University Press

movements by 2020[1], requires reconsideration of the current use of the noise budget. Furthermore, the Dutch government is currently considering a replacement of the current system based on enforcement points with a population-based system limiting the total number of people or houses within a specified noise contour. These two developments may allow for site-specific, population-based noise abatement procedures to be developed, to maximise the number of movements within the noise budget.

Research into the field of noise abatement procedures has been quite extensive in recent years; Clarke *et al*[2] and Van Boven[3] both studied continuous descent approaches (CDA) – possibly in combination with reduced flap settings and increased ILS glide slope angles – resulting in a consistent reduction of the noise impact on local communities. For departure procedures, Erkelens[4] proposed the use of area navigation (RNAV) to design precision navigation instrument departures (PNID) in order to reduce the flight track dispersion and allow for more lateral freedom in the trajectory design. Finally, Prats *et al*[5] used 4D optimisation techniques to numerically optimise flight trajectories with respect to noise, based on fuzzy logic and using RNAV.

Another, more recent issue for civil aviation is the environmental impact of gaseous emissions. Although the current regulations which apply at Dutch airports do not yet limit the growth of civil aviation, the need to consider the impact of these emissions on near-airport communities is still increasing. Work done in the framework of the European ExternE[6] project offered a possibility to express the damage caused by gaseous pollutants on the human environment in terms of monetary values. With regard to the reduction of aviation emissions, Antoine *et al*[7] studied the possibility to apply optimisation techniques in the conceptual design phase of modern airliners to reduce their environmental impact – of both noise and pollutant emissions – at a minimal increase in operating costs. The need for minimal increased operating costs is supported by Brooker[8], who concludes that in spite of the increased public awareness of the environmental impact of civil aviation, the priority in aircraft design should still be reduction of the operating costs.

Previous research has shown several approaches to assess and reduce the environmental impact of civil aviation in the vicinity of airports. The aim of this study is to combine a number of these approaches into one software tool for the design of departure procedures and, more specifically, standard instrument departures (SID). To optimise trajectories with respect to site-specific noise impact criteria, Delft University of Technology has developed the tool NOISHHH[9-12]. NOISHHH combines a noise model, a geographical information system (GIS), a dose-response relationship and a dynamic optimisation algorithm. For this study, NOISHHH has been adapted to enable it to design RNAV SIDs in which a trade-off can be made between environmental and operational cost criteria.

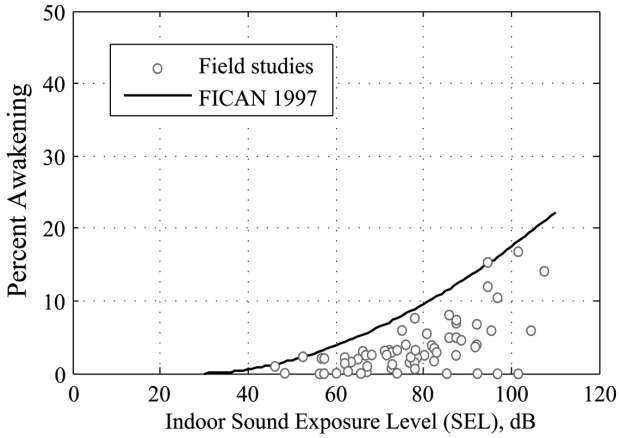

Figure 1. FICAN recommended sleep disturbance dose-response relationship.

NOISHHH has therefore been extended with an emissions model and made compliant with the regulations and guidelines which apply to SIDs and RNAV through the use of operational constraints.

To illustrate the capabilities of the new version of NOISHHH, two SIDs currently in use at AAS have been optimised with respect to noise and pollutant emissions using a Boeing 737-300 aircraft model.

The outline of this paper is as follows. Section 2.0 describes the method of environmental optimisation. In Section 3.0, the aircraft performance modelling is discussed. The noise and emission modelling are then presented in Section 4.0. Section 5.0 offers the numerical methodology of the optimisation process, followed by two example scenarios in Section 6.0. Finally, the conclusions of the research are presented in Section 7.0.

2.0 ENVIRONMENTAL OPTIMISATION

Whilst the current noise abatement procedures at AAS and other airports have been designed to minimise specific contour areas, NOISHHH distinguishes itself by using site-specific, population-based noise optimisation criteria. Population density data are therefore made available in NOISHHH through the GIS to allow the tool to assess the total number of people affected by the noise impact. By directly basing noise abatement on the population density, NOISHHH can improve routing over less noise-sensitive areas and reduce the impact in the areas still affected by noise.

In addition, the new version of NOISHHH incorporates the assessment of gaseous pollutants. When gaseous pollutants are considered, two categories need to be distinguished: 1) global emissions, which concern large-scale effects such as global warming and acid rain and 2) local emissions, which concern the direct impact of emissions on, for instance, human health and the human environment. For this study, which only assesses the impact of aviation emissions on near-airport communities, only local emissions have been considered. These are defined as pollutants emitted below the mixing height of 3,000ft (915m). The four pollutants considered in this research are carbon monoxide (CO), hydrocarbons (HC), sulphur oxides (SO_x) and nitrogen oxides (NO_x). These four have been selected as they have a direct impact on the human environment – a selection also supported by the European ExternE[6] project.

In order to optimise with respect to multiple environmental criteria and, more importantly, to be able to make a trade-off between environmental and operational cost considerations, a composite performance index has been defined which contains a weighted contribution of the optimisation criteria;

$$J = K_1 \cdot \int_{t_0}^{t_f} \sigma \, \mathrm{d}t + \sum_{n=2}^{5} K_n \cdot \int_{t_0}^{t_{3,000\,ft}} EI_n \cdot \sigma \, \mathrm{d}t + K_6 \cdot N_A \qquad \ldots (1)$$

where σ is the fuel flow in kg•s^{-1}, EI_n the emission index in g•kg^{-1} and N_A the upper bound to the number of people expected to awake due to a single night-time flyover. The weighting factors ($K_n \geq 0$) are cost coefficients. For fuel, K_1 is expressed in €•kg^{-1} and is based on the approximate cost of jet fuel at the time of this research (June 2008)[13]. The cost coefficients $K_{2\text{-}5}$ for emissions are based on research done in the scope of the European ExternE[6] project and are damage cost coefficients. These coefficients are derived from the economical damage to the human environment caused by gaseous pollutants and are also expressed in €•kg^{-1}. An overview of the cost coefficients for fuel and emissions can be found in Table 1. The impact of emissions is not site-specific as it does not take into account the population density below the flight path. Finally, for awakenings, the cost coefficient K_6 is expressed in €•awakening^{-1}. Since no value was available for this coefficient, it is parametrically varied to assess the impact of awakenings on

https://doi.org/10.1017/S0001924000004243 Published online by Cambridge University Press

the trajectories. All optimisations are based on the assumption that the financial responsibility for the external damage costs is assigned to the airlines.

Table 1
Cost coefficients for fuel and emissions

Performance criterion	Cost coefficient, €•kg^{-1}
Fuel, K_1	0·82
Hydrocarbons, K_2	1·867
Carbon monoxide, K_3	$3{\cdot}2 \bullet 10^{-4}$
Nitrogen oxides, K_4	2·63
Sulphur oxides, K_5	6·49

As can be seen from Equation (1), the impact of noise is expressed as the number of expected awakenings due to a single night-time flyover. In order to determine this number, a dose-response relationship between the noise exposure and the expected percentage of awakenings is combined with the population density data in the GIS. The dose-response relationship is based on research done by the Federal Interagency Committee on Aviation Noise (FICAN) in 1997[14]. The resulting relationship, as shown in Fig. 1, is based on laboratory tests and field experiments and provides an upper bound to the expected number of awakenings;

$$\%Awakenings = 0{\cdot}0087 \cdot (SEL_{indoor} - 30)^{1{\cdot}79} \quad \ldots (2)$$

where SEL_{indoor} represents the indoor A-weighted sound exposure level (SEL) in dBA. The indoor SEL is found by correcting the outdoor SEL value for the average sound absorption of a typical house, which is 20·5 dBA[9-12]. The absolute number of people expected to be awoken can now be determined from Equation (2) and the population density data.

In order to calculate the noise impact on the ground, the population density data, i.e. the observer locations, have been divided into a grid. For each cell, the number of people is defined based on data obtained from the Dutch Central Bureau of Statistics (CBS). Since the overall size of the grid, in combination with the selected cell size, is of great influence on the numerical effort and therefore the computation time, a rather coarse mesh is used consisting of 1 × 1km cells. For the SIDs considered in this study, grids of respectively 80 × 80km and 50 × 50km have been used. Figure 2 provides an example of the population density data as used in this research.

3.0 AIRCRAFT PERFORMANCE MODELLING

The aircraft model used in the NOISHHH tool is an intermediate point-mass model of a Boeing 737-300, with the assumptions that 1) there is no wind vector present, 2) the Earth is flat and non-rotating and 3) the flight is coordinated. All calculations are performed in standard atmospheric conditions. Furthermore, the flight path angle is considered sufficiently small ($\gamma < 15^o$) and the weight is considered constant throughout the departure procedure. The equations of motion are now defined as;

$$\begin{aligned} \dot{x} &= V \cdot \mathrm{Cos}\gamma \cdot \mathrm{Sin}\chi \\ \dot{y} &= V \cdot \mathrm{Cos}\gamma \cdot \mathrm{Cos}\chi \\ \dot{h} &= V \cdot \mathrm{Sin}\gamma \\ \dot{\chi} &= \frac{g_0 \cdot \mathrm{Tan}\mu}{V} \\ \dot{E} &= \frac{V \cdot (T - D)}{W} \end{aligned} \quad \ldots (3)$$

The aircraft is controlled by the flight path angle γ, the bank angle μ and a relative thrust setting Γ. The latter is defined as;

$$\Gamma = \frac{T - T_{\min}}{T_{\max} - T_{\min}} \quad \ldots (4)$$

The design of RNAV SIDs is liable to a number of operational constraints[15,16]. In principle, RNAV allows for more lateral freedom of movement within a network of navigational beacons. However, for the specific case of noise abatement, reduction of the flight track dispersion is beneficial and therefore two specific leg types are recommended. They are the track to a fix (TF) leg and the radius to a fix (RF) leg, which define a straight track and a constant radius turn between two fixes respectively. The use of the desired leg types can be ensured by introducing two new constraints, *viz*, one for TF legs to disallow banking, and one for RF legs to impose a constant turn radius;

$$\mu = 0$$
$$\frac{dR}{dt} = \frac{d}{dt}\left[\frac{V^2}{g_0 \cdot \mathrm{Tan}\mu}\right] = 0 \quad \ldots (5)$$

This approach does, however, require the turn radius R as an additional state, replacing the bank angle μ. Implementing the trivial differential equation $dR/dt = 0$ in an RF segment ensures that the turn radius remains constant and equal to the boundary value of the RF segment. This approach essentially renders the radius R of each RF segment a parameter to be optimised. Using Equation (5), the bank angle follows from the turn radius and the airspeed. Constraints on the bank angle and the airspeed implicitly define the lower and upper limits for the turn radius;

$$\frac{V_{\min}^2}{g_0 \cdot \mathrm{Tan}\mu_{\max}} \le R \le \frac{V_{\max}^2}{g_0 \cdot \mathrm{Tan}\mu_{\min}} \quad \ldots (6)$$

For the specific case of RNAV SIDs, the maximum permissible bank angle ranges from 15º to 25º, increasing stepwise between 125m and 915m above field elevation (AFE)[15]. Below 125m AFE, no turning is allowed and a minimum bank angle limit of 10º is imposed in each RF segment.

Additionally, for obstacle clearance, a minimum procedure design gradient (PDG)[15] is defined at 3·3%. The PDG defines a plane in space starting from a point 5m above the end of the runway surface suitable for take-off, the so-called departure end of

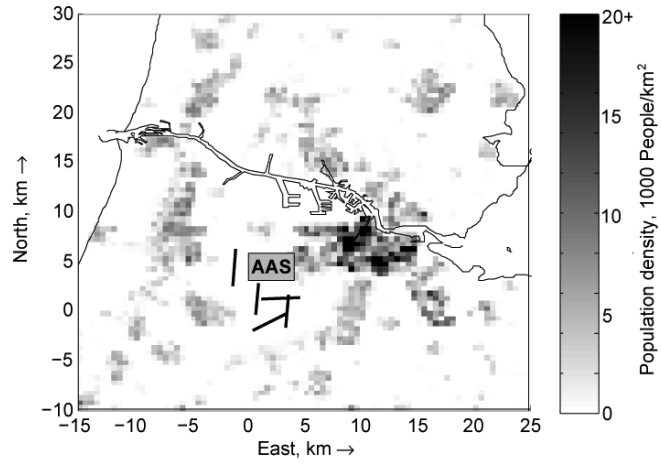

Figure 2. Population density in the vicinity of *AAS*.

https://doi.org/10.1017/S0001924000004243 Published online by Cambridge University Press

the runway (DER). This implies that from the DER, the altitude gained divided by the ground distance travelled must always exceed 3·3%, assuming that no obstacles are present in the flight path. To account for a take-off prior to the DER on a sufficiently long runway for the medium-sized Boeing 737-300, the following constraint can be defined;

$$\frac{h - h_{DER} + PDG \cdot d_{DER}}{s} \geq PDG_{min} \quad \ldots (7)$$

where h_{DER} = 5m is the height of the DER above the runway, d_{DER} is the distance between the DER and the actual point of take-off (in this study 1,000m) and s is the ground track distance covered from the take-off point. The latter can be derived from;

$$\dot{s} = V \cdot \mathrm{Cos}\gamma \quad \ldots (8)$$

Thirdly, for the design of noise abatement procedures, deep thrust cutback offers the possibility to reduce thrust momentarily over highly noise-sensitive areas. The main restriction for these procedures is that below 3,000ft (915m) or before transition to en-route climb configuration – whichever occurs first – the thrust may not be reduced further than a level sufficient to comply with the climb gradients defined in FAR 25·111(c)[17]. This implies that in case of an engine failure the remaining thrust should be sufficient to maintain a climb gradient of 1·2% for twin-engine aircraft, assuming no automatic thrust restoration system (ATRS) is available. For this research, an ATRS is not assumed to be available. Based on the maximum available climb angle, the following inequality constraint can now be defined;

$$\mathrm{Sin}^{-1}\left(\frac{\frac{1}{2}T - D - \Delta D}{W}\right) \geq \gamma_{\mathrm{FAR}} \quad \ldots (9)$$

where ΔD represents the drag increment due to windmilling of the inoperative engine and additional control surface deflection to counter the asymmetrical thrust and drag forces.

Finally, some operational constraints are in effect at AAS: below 10,000ft a maximum Indicated Airspeed of 250kt is defined, as well as a maximum initial altitude of 6,000ft during departure procedures. In order to simplify the computational process, the indicated airspeed constraint has been replaced by a maximum equivalent airspeed of 250kt in this study. In view of the fact that during climb-out both speed and altitude remain relatively low, the error incurred due to this simplification is marginal. In addition, during departures NOISHHH does not allow the aircraft to descend or to decelerate.

An overview of all operational constraints can be seen in Table 2.

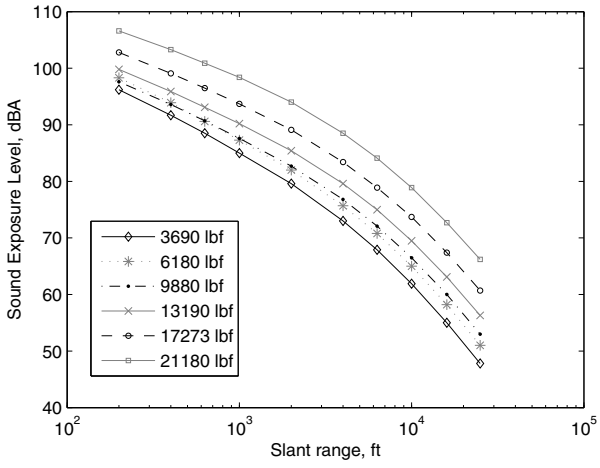

Figure 3. NPD-curves for the Boeing 737-300.

Table 2
Operational constraints for NOISHHH

Constraint	Definition
Maximum airspeed	$V_{eq} \leq V_{eq_{\max}}$
Maximum altitude	$h \leq h_{\max}$
No decelerations allowed	$\frac{\mathrm{d}V_{eq}}{\mathrm{d}t} = \frac{\mathrm{d}V}{\mathrm{d}t} \cdot \rho + \frac{1}{2} \cdot \frac{\mathrm{d}\rho}{\mathrm{d}h} \cdot \frac{\mathrm{d}h}{\mathrm{d}t} \geq 0$
No descents allowed	$\frac{\mathrm{d}h}{\mathrm{d}t} = V \cdot \mathrm{Sin}\,\gamma \geq 0$
Procedure Design Gradient	$\frac{(h - h_{DER} + PDG \cdot d_{DER})}{s} \geq PDG_{min}$
Turn radius	$\frac{V_{\min}^2}{g_0 \cdot \mathrm{Tan}\,\mu_{\max}} \leq R \leq \frac{V_{\max}^2}{g_0 \cdot \mathrm{Tan}\,\mu_{\min}}$
Thrust cutback	$\mathrm{Sin}^{-1}\left(\frac{\frac{1}{2}T - D - \Delta D}{W}\right) \geq \gamma_{FAR}$
Straight legs	$\mu = 0$
Constant radius turns	$\frac{dR}{dt} = \frac{d}{dt}\left[\frac{V^2}{g_0 \cdot \mathrm{Tan}\,\mu}\right] = 0$

4.0 NOISE AND EMISSION MODELLING

The noise model used in NOISHHH is derived from the Integrated Noise Model (INM) version 6.2 and is a direct replication of the noise engine incorporated in INM[18]. INM has been the Federal Aviation Authorities' standard noise assessment methodology since 1978. It provides several noise metrics for a wide range of modern transport aircraft to assess the noise impact of airports on their surroundings. The INM noise model uses segmented flight paths to approximate continuous trajectories. This feature makes the model specifically suitable to be used in NOISHHH as the optimisation technique used in it also discretises the trajectory into segments.

To find the noise impact at a specific observer location, INM uses noise-power-distance (NPD) tables from which the selected noise metric can be found through interpolation over the slant range and the net corrected thrust. For the Boeing 737-300 with two CFM56-3B1 engines, the NPD-tables have been visualised in Fig. 3. The tables are based on the assumption that the observer is standing directly below an aircraft passing in an infinitely long straight segment at a given reference speed. To correct for non-reference conditions, three adjustments are introduced: 1) the noise fraction adjustment, which accounts for finite length segments, 2) the duration adjustment, which accounts for non-reference speeds for exposure based metrics such as SEL and 3) the lateral attenuation adjustment, which corrects for ground reflection and refraction, for observers not positioned directly below the flight path.

The emissions model used in this study is the Boeing method 2 (BM2)[19], which offers a number of corrections to the International Civil Aviation Organization (ICAO) Engine Emission Databank[20]. This databank contains test data for a large number of modern jet engines. The emission indices of a number of gaseous pollutants, expressed in grams of pollutant per kilogram of fuel burnt, are available for four thrust settings representing taxiing, take-off, climb-out and arrival, thus enabling the assessment of a full landing and take-off cycle. Of the four gaseous pollutants considered in this study, CO, HC and NO_x are derived from the Engine Emissions Databank, whereas SO_x-emissions can be directly derived from the mass percentage of sulphur in jet fuel.

https://doi.org/10.1017/S0001924000004243 Published online by Cambridge University Press

The data available from the databank are only valid for test conditions. To account for atmospheric conditions and intermediate thrust settings, the data have to be corrected. For that purpose, the use of the Engine Emissions Databank is augmented with the Boeing method 2. This method provides a means for interpolating and correcting the data derived from the databank and consists of four basic steps. These steps include a correction for atmospheric conditions, airspeed and engine installation effects to the fuel flow (following from the Boeing 737-300 aircraft model), an interpolation of the ICAO data and a correction to the emission indices found. The fourth and final step determines the total emission of a single trajectory.

5.0 NUMERICAL METHODOLOGY

The NOISHHH tool uses the direct trajectory optimisation technique of collocation with nonlinear programming (NLP). This method transforms an optimal control problem into an NLP problem by discretising the trajectory dynamics[9-12]. In this process, the total time interval of an optimal control problem is divided into a number of subintervals, which are connected at so-called nodes. The values of the states and controls at these nodes are then treated as a set of NLP variables. The cost function and the system differential equations are discretised as well and transformed into algebraic equations (implicit integration). Finally, the state and control constraints are treated as algebraic inequalities in the corresponding NLP problem. The optimisation software used to solve the optimal control problem, called EZOpt[9-12], uses piecewise constant control histories and piecewise linear state histories. As mentioned before, this segmentation makes the INM noise model particularly suitable to be implemented in NOISHHH.

The number of nodes chosen to define the trajectory, along with the number of grid cells for the noise calculation, is of great influence on the computational burden of the problem. Depending on the complexity of the trajectory, the number of nodes can be varied. For this research, the departures have been modelled by 18 to 26 nodes. This approach ensures that in general full convergence of the problem is achieved in approximately one hour on a 2·10GHz laptop computer.

The optimisation method used in NOISHHH also allows for the use of a multi-phase problem definition. This is required to allow for discontinuous transitions in the state, control or constraint vector, which is, for instance, required to distinguish between straight legs and constant radius turns. To ensure a smooth transition between two consecutive phases, event constraints can be used, where an event describes the connection between two phases. A downside to the use of multiple phases, however, is that the sequence of the phases must be predefined in the initial guess. A suitable initial guess must contain a feasible trajectory estimate and is usually created through the graphical user interface of EZOpt, either from scratch or by using a previous solution. The result of an erroneous identification of the phase sequence in this file could be that the optimal solution found for the problem as posed in NOISHHH may not be the actual optimal solution for the problem intended. In the example scenarios, for instance, the aircraft is allowed to turn before, during or after retracting flaps. Since each consecutive flap setting and the transition from straight legs to turns requires an event, the predefined order of phases and events might require a large number of initial guesses and, as a result, a large number of calculation runs. In this study, additional phases were also required for bank angle constraints, costs of emissions and the thrust cutback constraint, rendering it very difficult to find the correct order of the phases. In order to overcome this problem, the number of phases has been reduced by replacing a number of discontinuous transitions by continuous approximations, eliminating the need for additional phases and thus reducing the combinatorial problem.

In the original version of NOISHHH, the flap retraction schedule was implemented as a set of quadratic polynomials, each representing a specific drag polar corresponding to a specific aircraft configuration. For the aircraft under consideration in this study, it is feasible to combine the four polynomials used in the departure trajectory by one single quadratic polynomial enveloping all aircraft configurations used. It is assumed that the small error introduced by approximation of the four polynomials outweighs the disadvantages of using the discrete steps as used in the original version of NOISHHH.

For the costs of emissions, bank angle constraints and the thrust cutback constraint, four additional events would be required. For all these events, so-called switch functions have been introduced to further eliminate the need for additional phases. These functions, based on the arctangent function, form a good representation of the otherwise stepwise change in the cost or constraint vectors. Furthermore, the functions are twice differentiable, which is beneficial for the robustness of the optimisation algorithm. The basic form of the functions used is;

$$sw(y) = \alpha \cdot \mathrm{Tan}^{-1}\left(\frac{\beta}{y_{sw}} \cdot y - \beta\right) + \zeta \qquad \ldots (10)$$

where y_{sw} defines the switching point, α and ζ define the starting point and the amplitude and β defines the gradient of the function. The latter is specifically important, since a steep gradient results in a more accurate approximation of the stepwise change, but adversely affects the robustness of the optimisation tool. When a value for β has been selected, the values for α and ζ directly follow from the requirements of the switch function.

As a first example, the costs of emissions are considered. These costs only contribute to the performance index below 3,000ft (915m). This implies that at 3,000ft an event would be required to change the performance index. This can, however, be avoided by replacing the costs of emissions in Equation (1) by;

$$J_{em} = \sum_{n=2}^{5} K_n \cdot \int_{t_0}^{3{,}000\,ft} EI_n \cdot \sigma \, dt = sw_{em} \cdot \sum_{n=2}^{5} K_n \cdot \int_{t_0}^{t_f} EI_n \cdot \sigma \, dt$$

$$sw_{em} = \begin{cases} 1, & h \le 3{,}000\ ft \\ 0, & h > 3{,}000\ ft \end{cases} \approx \left(\frac{-0{\cdot}5}{\mathrm{Tan}^{-1}(60)} \cdot \mathrm{Tan}^{-1}\left\{ \frac{60}{915} \cdot h - 60 \right\} + 0{\cdot}5 \right) \qquad \ldots (11)$$

This approach results in the costs of emissions only being taken into account below 3,000ft as a result of the arctangent function, which is of the form as expressed by Equation (10). A similar approach can be used for the maximum bank angle and the thrust cutback constraint defined in Equation (9). However, in both cases two different switch points occur. Firstly, for the maximum bank angle, which starts at 15º and changes to 20º at 305m and to 25º at 915m, two switch functions are added and then used to define the maximum bank angle;

$$\mu_{\max_1} = \frac{5}{2 \cdot \mathrm{Tan}^{-1}(60)} \cdot \mathrm{Tan}^{-1}\left(\frac{60}{305} \cdot h - 60 \right) + 17 \cdot 5$$

$$\mu_{\max_2} = \frac{5}{2 \cdot \mathrm{Tan}^{-1}(180)} \cdot \mathrm{Tan}^{-1}\left(\frac{60}{915} \cdot h - 180 \right) + 2 \cdot 5$$

$$\mu_{\max} = \mu_{\max_1} + \mu_{\max_2} \qquad \ldots (12)$$

It should be noted that the fact that turning is not allowed below 125m is covered by the constraint for the first phase – a straight leg – to end at or above 125m.

Secondly, the thrust cutback constraint requires not two consecutive, but two parallel switch points. Above 3,000ft (915m) or when the aircraft is in a clean configuration – in this case above 190kts TAS – the constraint is no longer active. For this constraint a

https://doi.org/10.1017/S0001924000004243 Published online by Cambridge University Press

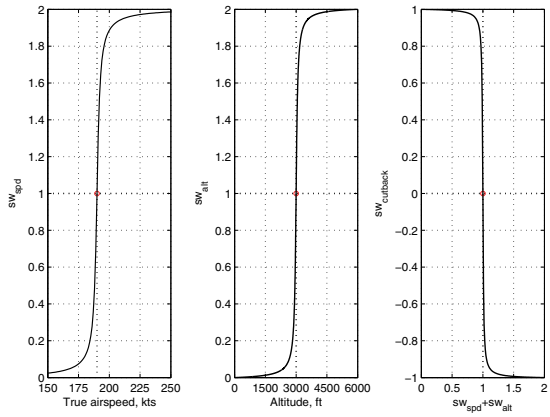

Figure 4. Switch functions for the thrust cutback constraint.

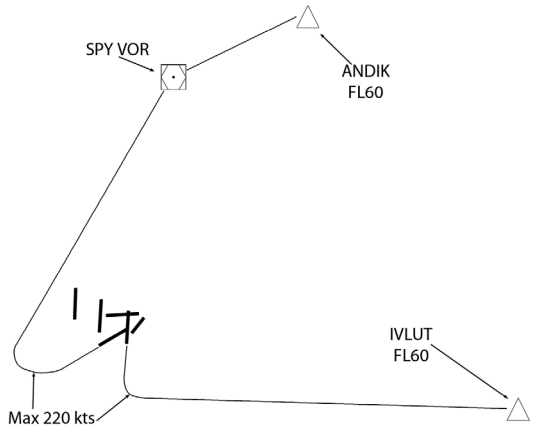

Figure 5. Spijkerboor and *ARNEM SIDs*.

composite switch function is defined in which two separate functions are used as the input to a third composite switch function;

$$sw_{spd} = \frac{1}{\mathrm{Tan}^{-1}(100)} \cdot \mathrm{Tan}^{-1}\left(\frac{100}{190} \cdot V - 100\right) + 1$$

$$sw_{alt} = \frac{1}{\mathrm{Tan}^{-1}(50)} \cdot \mathrm{Tan}^{-1}\left(\frac{50}{915} \cdot h - 50\right) + 1$$

$$sw_{cutback} = -\frac{1}{\mathrm{Tan}^{-1}(100)} \cdot \mathrm{Tan}^{-1}\left(100 \cdot \left[sw_{spd} + sw_{alt}\right] - 100\right) \quad \ldots (13)$$

As an example of the use of switch functions the latter, most elaborate of the three functions, has been visualised in Fig. 4.

Now, when one of the switch points is reached, the composite function switches to a value of $sw_{cutback} = -1$. This can be explained by looking at the resulting definition of the constraint expressed in Equation (9);

$$\mathrm{Sin}^{-1}\left[\frac{\left(\frac{N - sw_{cutback}}{N}\right) \cdot T - D - \Delta D}{W}\right] \geq \gamma_{\mathrm{FAR}} \quad \ldots (14)$$

where N is the number of engines. Before the switch point $sw_{cutback} = 1$, which results in the simulation of an inoperative engine. After the switch point has been passed, a fictional 'third' engine becomes available in the constraint. This is required since at this point the thrust can even be lowered to a level where two engines supply just enough thrust to maintain airspeed and altitude. So, at that point, no climb gradient is required, nor is the drag increment to be taken into account. The addition of a surplus of thrust resulting from the third engine renders the constraint inactive and allows the aircraft to fly level at constant airspeed.

Although the use of switch functions introduces an error close to the switch points, it is assumed that the overall error is negligible, since the errors are symmetrical at the switch point. The errors introduced again outweigh the disadvantages of using a large number of phases.

After the introduction of the switch functions, along with the quadratic approximation of the flap schedule, phases are only required to distinguish between straight legs and constant radius turns, as well as the transition between take-off and climb thrust. The exact location within the order of the TF- and RF-legs for this transition needs to be determined. However, since a non-RNAV constrained solution is always used as the initial guess to the RNAV solution, the approximate location of this transition point can be easily determined.

6.0 RESULTS

6.1 Example scenarios

To show the functionality of the adapted tool, two SIDs currently in use at AAS have been used as a base to find their optimal equivalents. These departures, the so-called Spijkerboor departure from runway 24 and the ARNEM departure from runway 18L[21], cause a significant noise impact in the communities of Hoofddorp, Nieuw-Vennep, Haarlem, Aalsmeer and Uithoorn (see Fig. 17). Both current procedures are presented in Fig. 5. For both departures, the optimised trajectory starts at 5m AFE and at 1,000m before the end of the runway. The Spijkerboor optimisation ends at the ANDIK intersection and the ARNEM optimisation ends at the IVLUT intersection, both at FL60.

As a first step in finding the optimal solution, the current SIDs have been used to create a rough initial guess to the non-RNAV constrained problem as implemented in the original version of NOISHHH. The converged optimal solution obtained for this non-RNAV problem is then used to synthesise an initial guess for the RNAV constrained trajectory optimisation problem as considered in the adapted version of NOISHHH. This new initial guess is essentially obtained by approximating the non-RNAV optimal solution in terms of a sequence of straight (TF) legs and constant radius (RF) turns. In the RNAV adapted version of NOISHHH the identified route structure is then employed to set up a multi-phase formulation, where in each phase the appropriate RNAV constraints corresponding to one of the identified (TF or RF) RNAV legs are implemented. The length of each TF leg as well as the circular arc and turn radius of each RF leg (and thus the location of the events) is completely determined in the trajectory optimisation process.

This process can be seen in Fig. 6, in which the events are indicated by squares. The Spijkerboor departure consists of a straight leg climbing to at least 125m, a turn towards the North, followed by two straight legs connected by a short turn towards the ANDIK intersection. To get a clear view of the impact of emissions, noise is not considered in the performance index in the first optimisation runs. For that reason a simplified trajectory is used for Spijkerboor, where the last three phases are replaced by a single straight leg leading directly to the ANDIK intersection.

https://doi.org/10.1017/S0001924000004243 Published online by Cambridge University Press

To validate the impact of the optimisation, the ARNEM departure has been selected. This departure is less complicated in terms of the number of heading changes and can therefore offer an insight into the impact of lateral changes in the trajectory. Furthermore, it poses a significantly different noise problem due to a different population distribution beneath the flight path. This departure only consists of a straight leg to climb to at least 125m, followed by a single turn and a final straight connection to the IVLUT intersection.

The results of both optimised departure trajectories are compared to an ICAO-A departure[22] – the standard procedure at AAS – using the current SIDs. This departure procedure was originally designed to minimise the noise impact on close-in communities, and mainly focuses on climbing as fast as possible, while accelerating only upon reaching 3,000ft.

6.2 Numerical results

6.2.1 Spijkerboor departure

Firstly, an optimised solution for fuel only was computed, which was then used as an initial guess for the composite emissions- and fuel-optimised solution. It was found that both solutions are very similar, which can be seen from the results presented in Table 3. These results can easily be explained by considering that the contribution of the emissions to the total performance index is only minor ($J_{em} \approx 0{\cdot}02\ J$). This is a direct result of the relatively low cost coefficients for the gaseous pollutants used in this research (see Table 1). Furthermore, optimising with respect to fuel might also result in significantly reduced emissions as compared to standard procedures, due to the direct link between fuel burn and emissions.

To further evaluate the impact of the cost coefficients used for emissions on the trajectory and the total fuel burn, a set of additional optimisations has been executed, with increased values for the cost coefficients $K_{2\text{-}5}$. To be able to assess a solution in which emissions are dominant in the performance index, the cost coefficients for emissions were multiplied up to 100 times. It should be noted that the part of the trajectory above 3,000ft is still optimised only for fuel. The results are presented in Fig. 7, in which all results are normalised with respect to the fuel-optimised solution.

From these results it can be seen that in the emissions-optimised solution the total costs of gaseous pollutants can be reduced by about 17%, at the expense of a 5% increase in the total fuel cost. More importantly, the dominance of NO_x-emissions in the performance index can clearly be distinguished. The total emissions and the emission of NO_x are closely related and the NO_x-emission is reduced at the expense of increasing HC, CO and SO_x for high cost coefficients. However, notwithstanding the dominance of NO_x, the other gaseous pollutants are also reduced by about 10% for higher cost coefficients. As a final comparison, Figs 8 and 9 present the (partial) altitude and airspeed histories of the fuel-optimised and the emissions-optimised trajectories.

These figures clearly show the difference in behaviour for both trajectories. In the fuel-optimised trajectory, the emphasis lies more on accelerating and climbing, yielding a significantly higher total energy upon reaching 3,000ft compared to the emissions-optimised solution. From approximately 20 to 110 seconds, the emissions-

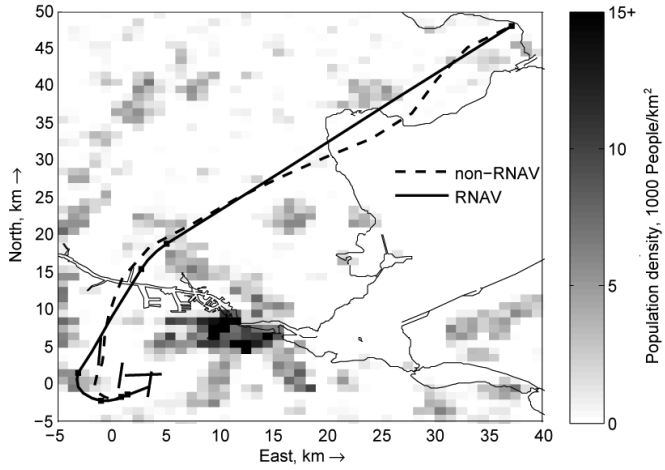

Figure 6. RNAV approximation.

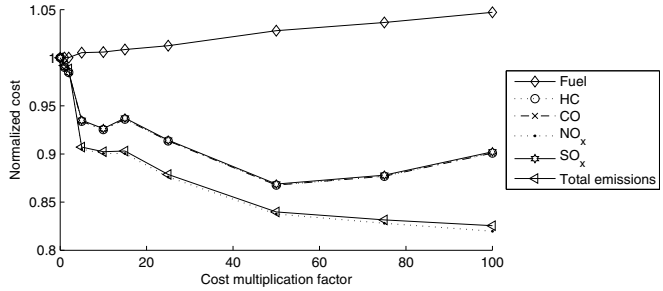

Figure 7. Influence of increased emissions cost coefficients.

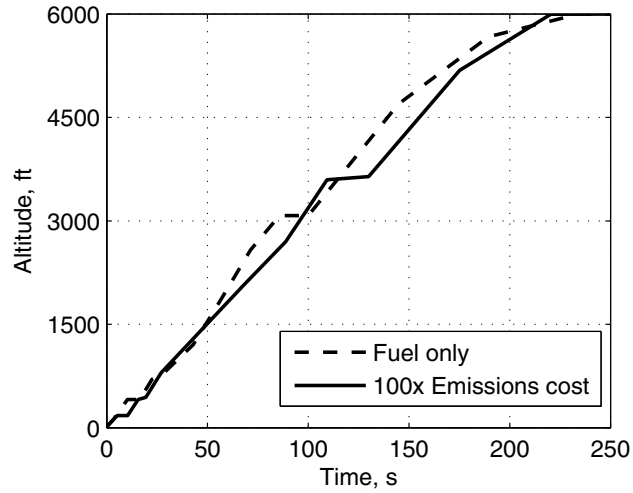

Figure 8. Altitude history, fuel and emissions.

Table 3
Results of the fuel- and emissions-optimised Spijkerboor departure

Optimisation		Fuel, kg	HC, g	CO, g	NO_x, kg	SO_x, g	Emissions	Total
Fuel	Mass	523	7·00	144	2·54	76·2		
	Cost	€429·84	€0·01	€0·00	€6·69	€0·49	€7·20	€437·04
Composite	Mass	523	6·87	141	2·51	74·8		
	Cost	€429·64	€0·01	€0·00	€6·61	€0·49	€7·11	€436·75

https://doi.org/10.1017/S0001924000004243 Published online by Cambridge University Press

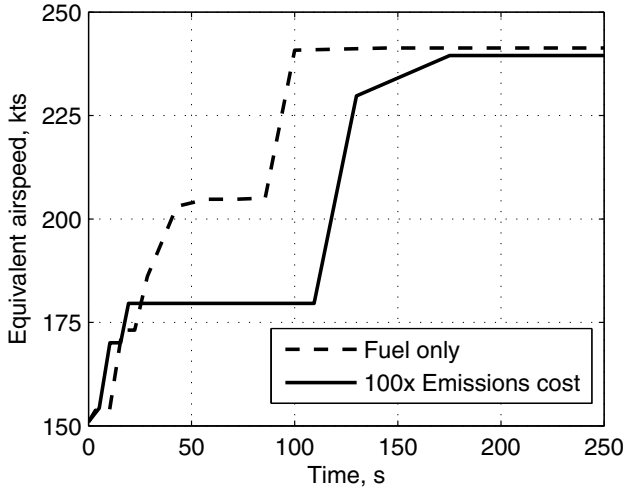

Figure 9. Airspeed history, fuel and emissions.

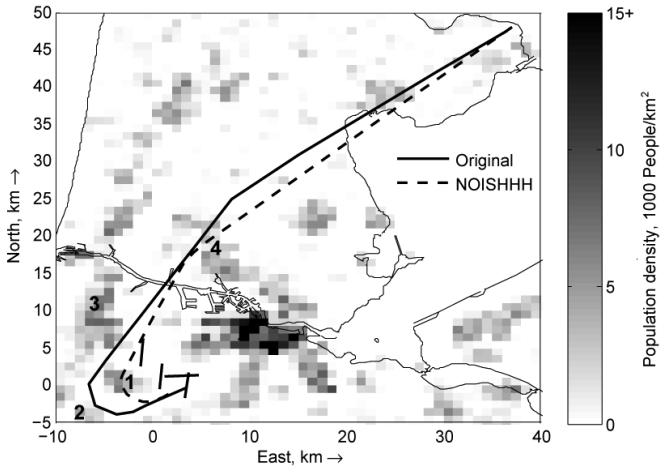

Figure 10. Noise-optimised Spijkerboor departure.

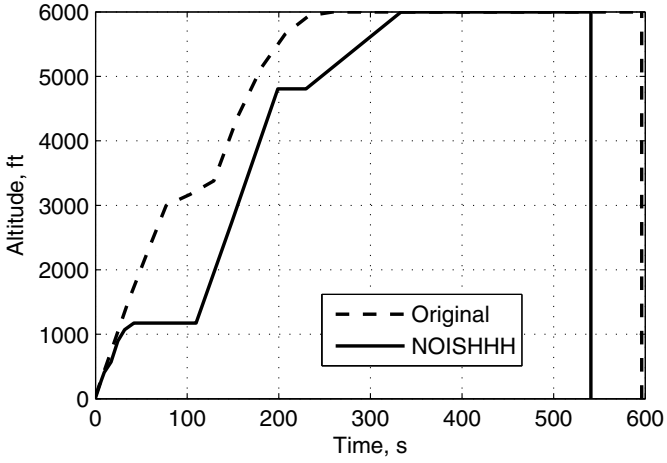

Figure 11. Altitude history, Spijkerboor.

optimised trajectory maintains an equivalent airspeed of 180kts, which indicates that the aircraft is not fully cleaned up. Furthermore, the emissions-optimised trajectory only reaches 3,000ft about 12 seconds later than the fuel-optimised solution. In this part of the trajectory, the emissions-optimised solution has a 20% lower throttle setting relative to the fuel-optimised solution. This results in a 15% increase in time-to-climb to 3,000ft, but (in combination with the lower airspeed) also yields an approximate 30% decrease in the BM2-based NO_x mass flow, which is the dominant factor in the performance index. On the other hand, the fact that the emissions-optimised trajectory deviates from the fuel-optimised trajectory below 3,000ft logically results in a higher fuel burn over the entire trajectory.

However, since only the original cost coefficients result in a meaningful compromise between fuel and emissions and the resulting impact on the performance index is negligible, emissions have not been taken into further consideration in the noise trade-off study. In this study, multiple cost coefficients pertaining to noise have been evaluated in order to allow for a trade-off between noise and fuel burn. The resulting trajectories are also compared to an ICAO-A version of the original SID, which is fuel-optimised after an altitude of 3,000ft is passed. Table 4 compares the results in terms of the total number of awakenings between the fuel-optimised ICAO-A departure and the noise-optimised solution with the largest cost coefficient K_6 that has been considered. Larger values for K_6 showed no further significant improvements in the number of awakenings.

Table 4
Results for the noise-optimised Spijkerboor departure

Trajectory	Time, s	Fuel burn, kg	Awakenings
Original	596	581	5,297
$K_6 = 0{\cdot}05$	540	525	3,801

These results clearly show that a significant decrease in the number of awakenings is achieved in the noise-optimised solution relative to the reference solution. Moreover, the transit time and the total fuel burn are also reduced by about 10%. From Figs 10 and 17 the causes of these reductions can be explained. In the community of Hoofddorp (1), the total number of awakenings has increased with respect to the reference departure, caused by a short, slow and low turn over the north-eastern part of the city. As a result, however, the noise impact in the communities of Nieuw-Vennep (2), Haarlem (3) and Zaanstad (4) is greatly reduced, resulting in an overall 35% decrease in the number of awakenings. When the altitude histories in Fig. 11 are compared, it can be seen that in the optimised departure the aircraft climbs to around 1,200ft to allow for a bank angle of 20º, keeping the turn radius small. Over Hoofddorp a turn is executed at relatively low speed (~ 187kt EAS), at which the aircraft has just transitioned to a clean configuration. Only after Hoofddorp has been passed, the thrust is increased to climb to around 4,800ft, where again thrust is reduced and the aircraft levels off. At this point the trajectory passes Zaanstad, after which the final climb to 6,000ft is executed.

The throttle control and speed histories for both trajectories in Figs 12 and 13 can be used to explain the effect of the deep thrust cutback constraint. Up to about 32 seconds maximum take-off thrust is applied, the end of which is marked in the control history. After that, the ICAO-A departure remains at full throttle (Γ remains 1, indicating maximum climb thrust is applied), whereas the optimised departure reduces throttle to about 80% climb thrust to accelerate to 190kt TAS, required to retract the flaps and so to render the thrust cutback constraint inactive. This allows for a thrust reduction to about 35% of maximum climb thrust. This level is required to maintain altitude at 190kt TAS in the turn over Hoofddorp, but also results in a significant reduction of the noise impact. After Hoofddorp has been passed, thrust is again increased to accelerate and climb further. At around 200 seconds, a second, smaller thrust

https://doi.org/10.1017/S0001924000004243 Published online by Cambridge University Press

cutback is seen over the community of Zaanstad. It can be concluded that instead of limiting the total thrust cutback, the constraint results in an early acceleration to render the constraint inactive and allow for much deeper thrust cutbacks.

The reduction in the total fuel burn and the transit time can be explained by considering that the overall time to climb to 6,000ft and accelerate to 250kts EAS for both procedures is quite similar, whereas the total time and total distance of the departure are decreased by about 10%. Furthermore, the early transition to clean configuration for the noise-optimised departure (about 50 seconds earlier than ICAO-A) also leads to a reduction in the total fuel burn.

6.2.2 ARNEM Departure

For the ARNEM departure again only a noise-optimised solution is considered, due to negligible impact of emissions for the cost factors extracted from the ExternE[6] project. Again, solutions for a range of values for the cost coefficient K_6 have been evaluated; the noise-optimised solution corresponding to the largest value of K_6 that has been considered is presented in Table 5.

Table 5
Results for the noise-optimised ARNEM departure

Trajectory	Time, s	Fuel burn, kg	Awakenings
Original	306	386	2,722
$K_6 = 0{\cdot}05$	287	349	1,895

As with the Spijkerboor departure, a significant reduction in the number of awakenings of about 30% is achieved, in combination with a 6% decrease in transit time and 10% less fuel burnt. However, in contradiction to the Spijkerboor departure, the ground tracks of the original and the optimised trajectories are very similar, as can be seen from Fig. 17. This implies that the decrease in awakenings is mainly due to the departure procedure, i.e. the vertical and airspeed profile. When the altitude history in Fig. 14 is considered, a similar result as for the Spijkerboor departure can be seen. A distinct portion of the trajectory can be identified at which the aircraft remains at approximately 1,000ft to make the turn at a maximum bank angle of 20°. After completing the turn and passing the communities of Aalsmeer and Uithoorn, the aircraft directly climbs to FL60.

A closer inspection of the throttle control and airspeed histories in Figs 15 and 16 reveals the effect of site-specific optimisation. Once 190kt TAS is reached, the flaps are retracted and the thrust is cut back to 30% to pass over the communities of Aalsmeer and Uithoorn. This is followed by a large increase in the throttle setting at around 70 seconds to accelerate and climb to the final conditions, until at around 200 seconds the thrust can be reduced again to maintain these conditions.

To summarise, both departure procedures have been plotted on a Google Earth overview of the surrounding area of AAS in Fig. 17.

7.0 CONCLUSIONS

This research has shown the possibility of optimising SIDs based on RNAV with respect to multiple environmental criteria, applying trajectory optimisation methods using a composite performance index. For the optimisation technique used, the application of switch functions is a valid means to overcome the combinatorial problem caused by the requirement to sequence a large number of phases in the optimisation problem.

Optimising with respect to gaseous pollutants using the emissions cost coefficients defined for this study has not led to meaningful results. This can be attributed to the minor contribution of emissions to the performance index, which is a direct result of the relatively small cost coefficients used for emissions. Drastically

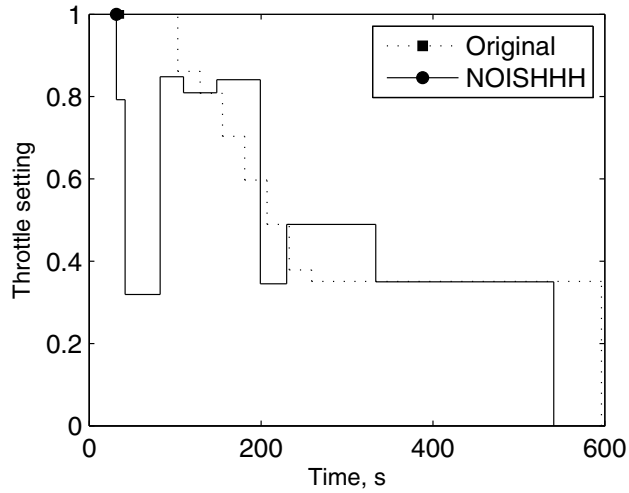

Figure 12. Throttle control history, Spijkerboor.

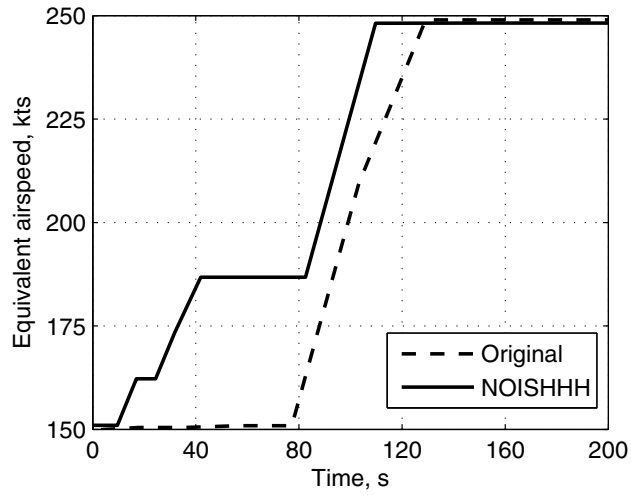

Figure 13. Airspeed history, Spijkerboor.

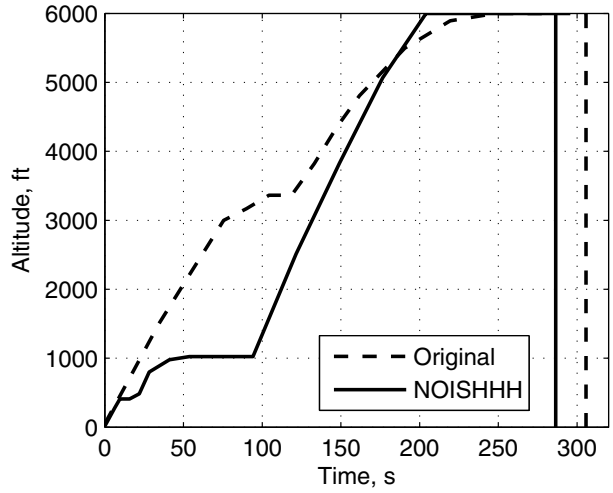

Figure 14. Altitude history, *ARNEM*.

https://doi.org/10.1017/S0001924000004243 Published online by Cambridge University Press

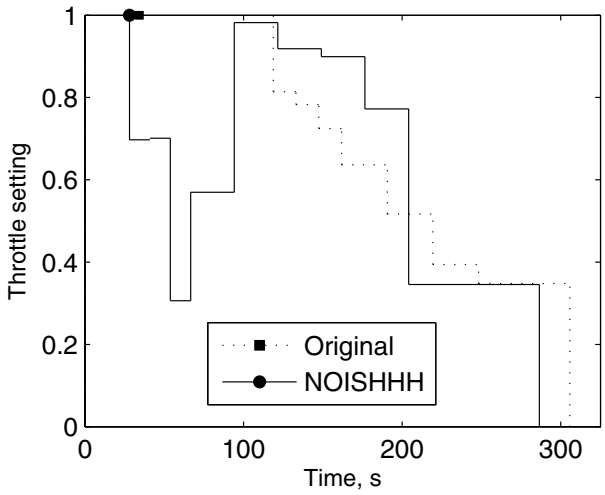

Figure 15. Throttle control history, *ARNEM*.

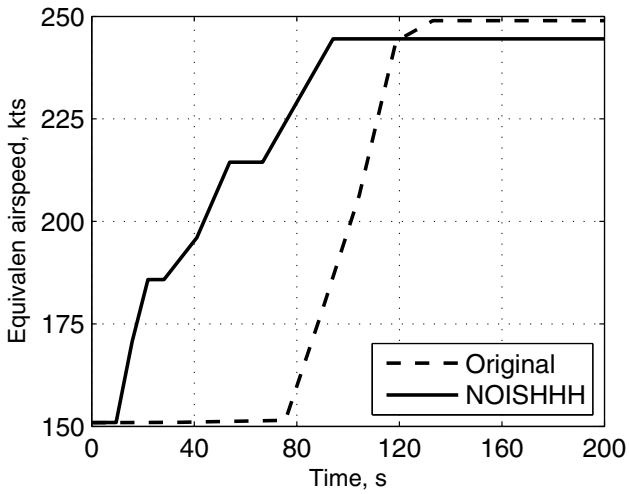

Figure 16. Airspeed history, *ARNEM*.

increasing these cost coefficients shows that the total amount of emissions can be significantly reduced, at the expense of only a minor increase in fuel cost. Due to the relatively large cost coefficient of NO_x and the total amount emitted, NO_x is clearly the dominant pollutant when optimising with the cost coefficients considered in this research.

Optimising with respect to the site-specific noise criterion of awakenings does lead to significant improvements in terms of noise impact. In addition, the optimised trajectories also result in a decrease in transit time and total fuel burn. When both departures considered in this research are examined, it can be concluded that the combined optimisation with respect to noise and fuel leads to a larger tendency towards early acceleration as compared to the standard ICAO-A procedure. In addition, it can be concluded that the departure procedure, i.e. the vertical path and the airspeed profile, is the main contributor to the reduction in the noise nuisance for the SIDs considered in this research.

Although the results attained in this study are very promising on the field of trajectory optimisation in general as well as on the field of the reduction of the environmental impact of civil aviation, further research is required. To assess the full capabilities of the newly designed tool, future research should focus on adding different aircraft types to the tool, and on including the effects of weather on both aircraft performance and environmental impact.

REFERENCES

1. ALDERS, H. Advies van de heer Alders over toekomst Schiphol en de regio tot 2010, Dutch Government Report, br.8977, June 2007.
2. CLARKE, J.P. and NHUT, T.H., *ET AL* Continuous Descent Approach: Design and Flight Test for Louisville International Airport, *J Aircr*, 2004, (41), **5**, pp 1054-1066.
3. VAN BOVEN, M. Development of Noise Abatement Approach Procedures, AIAA-2004-2810, 10th AIAA/CEAS Aeroacoustics Conference, Manchester, UK, 10-12 May 2004.
4. ERKELENS, L.J.J. Advanced Noise Abatement Procedures for Approach and Departure, AIAA-2002-4858, AIAA Guidance, Navigation and Control Conference and Exhibit, Monterey, CA, USA, 5-8 August 2002.
5. PRATS, X. and PUIG, V., *ET AL* Optimal Departure Aircraft Trajectories Minimising Population Annoyance, 3rd International Conference on Research in Air Transportation ICRAT, Fairfax, VA, USA, 1-4 June, 2008.

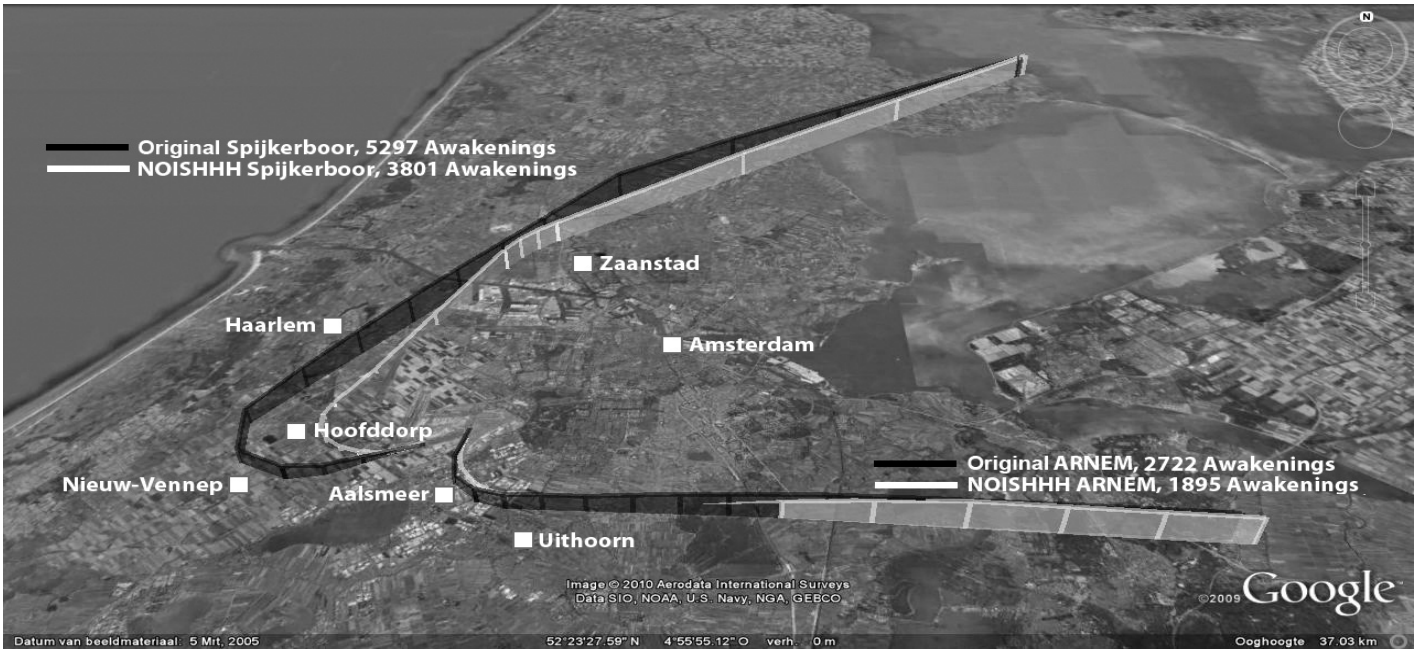

Figure 17. Original and noise-optimised *SIDs*.

https://doi.org/10.1017/S0001924000004243 Published online by Cambridge University Press

6. ExternE, Externalities of Energy, ExternE Methodology 2005 Update, 2005.
7. ANTOINE, N.E. and KROO, I.M. Aircraft optimization for minimal environmental impact, *J Aircr*, 2004, (41), **4**, pp 790-797.
8. BROOKER, P. Civil aircraft design priorities: air quality? climate change? noise?, *Aeronaut J*, 2006, **110**, (1110), pp 517-532.
9. VISSER, H.G. and WIJNEN, R.A.A. Optimisation of noise abatement arrival trajectories, *Aeronaut J*, 2003, **107**, (1076), pp 607-615.
10. VISSER, H.G. Generic and site-specific criteria in the optimisation of noise abatement trajectories, transportation Research Part D: Transport and Environment, 2005, (10), **5**, pp 405-419.
11. VISSER, H.G. and WIJNEN, R.A.A. Optimisation of noise abatement departure trajectories, 2001, *J Aircr, 2001*, **38**, (4), pp 620-627.
12. WIJNEN, R.A.A. and Visser, H.G. Optimal departure trajectories with respect to sleep disturbance, *Aerospace Science and Technology*, January 2003, **7**, pp 81-91.
13. International Air Transportation Association, Jet fuel price monitor, [online database], URL: http://www.iata.org/whatwedo/economics/fuel_monitor/index.htm [cited June 2008].
14. Federal Interagency Committee On Aviation Noise, Effects of aviation noise on awakenings From sleep, June 1997.
15. International Civil Aviation Organization, Procedures for Air Navigation Services – Aircraft Operations, ICAO doc nr. 8168, **II**, Construction of Visual and Instrument Flight Procedures, 5th ed, 2006.
16. European Organisation for the Safety of Air Navigation, Guidance Material for the Design of Terminal Procedures for Area Navigation (DME/DME, B-GNSS, Baro-VNAV & RNP-RNAV), 3rd ed, March 2003.
17. Federal Aviation Administration, Noise Abatement Departure Profiles, FAA Advisory Circular, 91-53a, July 1993.
18. BOEKER, E.R. and DINGES, E., *ET AL*, Integrated Noise Model (INM) Version 6.0 Technical Manual, FAA-AEE-02-01, U.S. Department of Transportation, 2006.
19. BAUGHCUM, S.L. and TRITZ, T.G., *ET AL*, Scheduled Civil Aircraft Emissions Inventories for 1992: Database Development and Analysis, Report NASA CR 4700, The Boeing Company, April 1996.
20. International Civil A viation Authority, ICAO Engine Exhaust Emissions Databank, Engine Exhaust Database [online database], URL: http://www.caa.co.uk/default.aspx?catid=702 [cited June 2008].
21. Aeronautical Information Services, Air Traffic Control The Netherlands, Aeronautical Information Publications [online database], URL: http://www.ais-netherlands.nl/aim/091105-091217/eAIP/html/index-en-GB.html [cited June 2008].
22. International Civil Aviation Organization, Procedures for Air Navigation Services – Aircraft Operations, ICAO doc nr. 8168, **I**, Flight Procedures, 5th ed, 2006.

https://doi.org/10.1017/S0001924000004243 Published online by Cambridge University Press